WSE
WATER SCIENCE AND ENGINEERING
HOHAI UNIVERSITY

http://www.waterjournal.cn
e-mail: wse2008@vip.163.com

Simulation algorithm for spiral case structure in hydropower station

Xin-yong XU*[1, 2], Zhen-yue MA[1], Hong-zhan ZHANG[1]

1. Faculty of Infrastructure Engineering, Dalian University of Technology, Dalian 116024, P. R. China
2. School of Hydraulic Engineering, North China University of Water Resources and Electric Power, Zhengzhou 450011, P. R. China

Abstract: In this study, the damage-plasticity model for concrete that was verified by the model experiment was used to calculate the damage to a spiral case structure based on the damage mechanics theory. The concrete structure surrounding the spiral case was simulated with a three-dimensional finite element model. Then, the distribution and evolution of the structural damage were studied. Based on investigation of the change of gap openings between the steel liner and concrete structure, the impact of the non-uniform variation of gaps on the load-bearing ratio between the steel liner and concrete structure was analyzed. The comparison of calculated results of the simplified and simulation algorithms shows that the simulation algorithm is a feasible option for the calculation of spiral case structures. In addition, the shell-spring model was introduced for optimization analysis, and the results were reasonable.

Key words: *hydraulic structure simulation; concrete damage-plasticity model; shell-spring model; spiral case*

1 Introduction

Recently, with the establishment of super-hydropower stations, such as the Three Gorges Project and Ertan Hydropower Project, spiral cases have become widely used in huge plants to maintain the internal pressure (Dong and Li 1995). An outstanding advantage of the spiral case is its adjustability to the load-bearing ratio between the steel liner and concrete via the variation of gaps in between (Li et al. 2004). The variation has been considered uniform in previous studies. However, under changing boundary conditions, the actual change of gaps is not uniform. Shen et al. (2008) performed simulation calculation based on the unevenness of gaps, and the result was confirmed by Xu et al. (2009). It is assumed that the effects of gaps and interactions between the steel liner and concrete cannot be eliminated when the water head reaches the value to maintain the internal pressure, and that the closing sequence of gaps also changes the load-bearing ratio between the steel liner and concrete. The interaction between

the steel liner and concrete is extremely complicated. However, this process can be clarified by using the simulation algorithm.

Several studies on the simulation algorithm have been performed. With further study and the increase of computational power, several models have been utilized to simulate the structural stress for spiral cases (Zhang et al. 2009). The model test and finite element method (FEM) were also employed to study the stress (Qin et al. 2002). By using the thermal stress method, Lin and Su (2001) studied the first-stage and second-stage concrete construction processes, focusing on the linear structural calculation.

Until now, research on the numerical calculation of spiral cases has mainly focused on the simulation analysis of the construction process, but a little research has been conducted on the structural damage. This is mainly due to the difficulty in combining the simulation algorithm with mechanics of materials for modeling concrete damages, which precludes the convergence in calculation of structural stresses (Shen et al. 2008).

Mazars (1985), Chaboche (1987), and Mazars and Pijaudier-Cabot (1989) put forward the methods of continuum damage mechanics. Ragueneau et al. (2000) and Burlion et al. (2000) analyzed the damage to concrete using the damage theory. Lubliner et al. (1989) proposed a damage-plasticity model for concrete, which was then modified and used by Lee and Fenves (1998) to simulate the concrete structure under cyclic loading, and the model was proven to be suitable for the hydraulic structure. Del Rio et al. (1987) suggested a three-dimensional finite element model for spiral cases. However, the study on the structure simulation of spiral cases with the damage-plasticity model has still not been conducted.

The damage-plasticity model verified by the model experiment was introduced to numerical simulation of damages during the construction and operational periods of spiral cases. A computational method based on the shell-spring model was also introduced to simulate the spiral case. An automatic computational program was successfully developed and verified, and can be used as an effective method in the scheme optimization.

2 Theoretic analysis

2.1 Damage-plasticity model

Based on mechanical theory, the damage-plasticity model was introduced to simulate the stiffness degradation and cracks of concrete (Lubliner et al. 1989; Lee and Fenves 1998). The irreversible damage variable was introduced to simulate the reduction of stiffness matrices of concrete based on continuum damage mechanics (HKSI 2002). The stress-strain relationship is defined as

$$\sigma = (1-d) D_0^{\text{el}} : (\varepsilon - \varepsilon^{\text{pl}}) = D^{\text{el}} : (\varepsilon - \varepsilon^{\text{pl}}) \tag{1}$$

where σ is the Cauchy stress; D_0^{el} is the initial stiffness of the structure without occurrence of damages; ε is the total strain; ε^{pl} is the plastic strain; D^{el} is the stiffness of the damaged structure, and $D^{\text{el}} = (1-d) D_0^{\text{el}}$; and d $(0 \le d \le 1)$ is the scalar damage factor. The reduction

of plastic stiffness can reflect the failure mechanism of concrete.

According to the continuum damage model, the effective stress can be expressed as

$$\bar{\sigma} = D_0^{\text{el}} : \left(\varepsilon - \varepsilon^{\text{pl}} \right) \tag{2}$$

The relationship between the Cauchy stress and effective stress can be expressed as

$$\sigma = (1 - d)\bar{\sigma} \tag{3}$$

For any section of the structure, the variable $1 - d$ represents the effective bearing rate, which is the ratio of the effective bearing area to the total area. When there is no damage, the effective stress equals the Cauchy stress. But when the structure is damaged, the effective stress $\bar{\sigma}$ is more reasonable for use in determining the damage. The damage factor d is controlled by the hardening variable $\tilde{\boldsymbol{\varepsilon}}^{\text{pl}}$ and effective stress $\bar{\sigma}$, i.e., $d = d\left(\bar{\sigma},\ \tilde{\boldsymbol{\varepsilon}}^{\text{pl}}\right)$.

The damage status of tension and compression can be characterized by the hardening variables $\tilde{\varepsilon}_t^{\text{pl}}$ and $\tilde{\varepsilon}_c^{\text{pl}}$, respectively, which are equivalent plastic strains. The equation of hardening variables can be expressed as

$$\tilde{\boldsymbol{\varepsilon}}^{\text{pl}} = \left[\tilde{\varepsilon}_t^{\text{pl}} \quad \tilde{\varepsilon}_c^{\text{pl}} \right]^{\text{T}} \tag{4}$$

The increase of microcracks in materials can be expressed by the change of hardening variables. The hardening variables are closely related to the energy dissipation, which leads to microcracks.

The yield function $F\left(\bar{\sigma},\ \tilde{\boldsymbol{\varepsilon}}^{\text{pl}}\right)$ expressed as the curved surfaces of the effective stress space, is used to determine the damage status. For the damage-plasticity model of the non-viscous materials, $F\left(\bar{\sigma},\ \tilde{\boldsymbol{\varepsilon}}^{\text{pl}}\right) \leq 0$. This model is suitable for the non-associated flow rules:

$$\dot{\varepsilon}^{\text{pl}} = \lambda \partial G\left(\bar{\sigma}\right) / \partial \bar{\sigma} \tag{5}$$

where $\dot{\varepsilon}^{\text{pl}}$ is the non-associated flow strain function, λ is a non-negative plastic factor, and G is a plastic potential function.

2.2 Shell-spring combined model

The complexity of the interaction between the steel liner and concrete depends on the nonlinear change of the gap in between. According to the characteristics of the structural cavity, the concrete just transfers loads in the radial direction. It can be summarized as elastic linkages that only constrain the normal displacement. With the development of the following method, the automatic analysis of the spiral case structure can be fulfilled.

The mechanical model of the shell-spring element is shown in Fig. 1, where i and j are two nodes. Certain parameters are defined as follows:
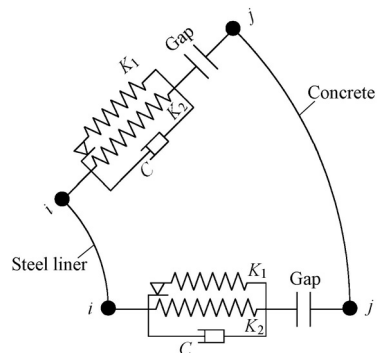

Fig. 1 Shell-spring model

the spring constants K_1 and K_2 are 22.0 MPa/cm, the damping coefficient C is a default value, and the gap varies from 0.3 cm to 1.8 cm. When the load is applied, the steel liner deforms outwards in the radial direction. Meanwhile, the distance between two nodes is gradually compressed, and the gap becomes smaller. After the gap completely disappears, the steel liner and concrete will bear the internal water pressure together.

3 Verification of damage-plasticity model

In order to verify the applicability of the damage-plasticity model in the simulation of spiral case structures, a laboratory model experiment was conducted to simulate the construction process of a spiral case, as shown in Fig. 2. The corresponding finite element model is shown in Fig. 3. As the surrounding concrete was filled, the load gradually increased to 2.8 MPa. The material properties of concrete specimens in the experiment are shown in Table 1. The loads and boundary conditions were applied according to the experimental situations.

Fig. 2 Laboratory model experiment
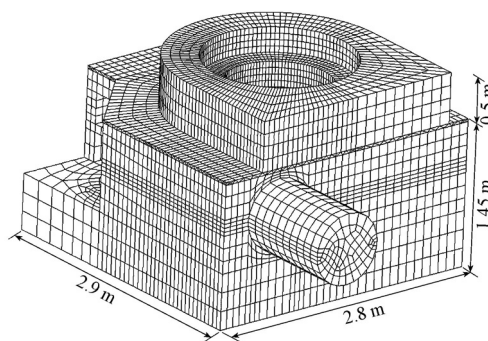

Fig. 3 FEM model for experimental spiral case

Table 1 Mechanical parameters of materials

| Material	Elastic modulus (GPa)	Poisson's ratio	Density (kg/m³)	Compressive strength (GPa)	Tensile strength (GPa)
Concrete (Experiment)	25.9	0.167	2 500	28.7	2.39
Concrete (Standard)	28.0	0.167	2 500	17.0	1.75
Spiral case	210	0.3	7 850	370	370
Dummy ring	210	0.3	7 850	205	205
Reinforcement	210	0.3	7 850	310	310

Two major concrete cracks in the model experiment, marked as L1 and L2, are shown in Fig. 4. They are located in the upper inlet portion of the model, and gradually extend from the outside of the intersection between the top of the spiral case and the concrete pier to the interior.

The plastic damage contour plot, which was obtained from the finite element model corresponding to the experimental situations, is shown in Fig. 5. The damage process and damage region are similar to those occurring in the experiment. The damage at the top extends

downstream as loads increase. The comparison between the experimental and simulated results shows that the damage-plasticity model for concrete is suitable for damage simulation of the spiral case structure.
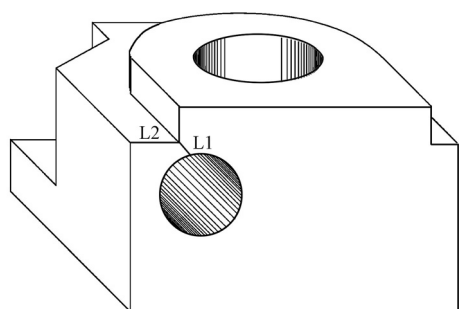

Fig. 4 Crack distribution of model experiment
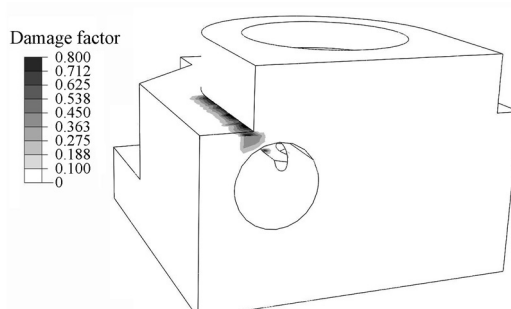
Fig. 5 Simulated results of damage to spiral case

4 Case study of simulation algorithm

4.1 Numerical model

The simulation algorithm was used to describe the construction process (Xu et al. 2009) and calculate the damage to a structure. The generator unit of a large power station was taken as a practical example in this study, and the numerical models were established as shown in Fig. 6 and Fig. 7. The construction process was simulated with the first-stage and second-stage concrete models.
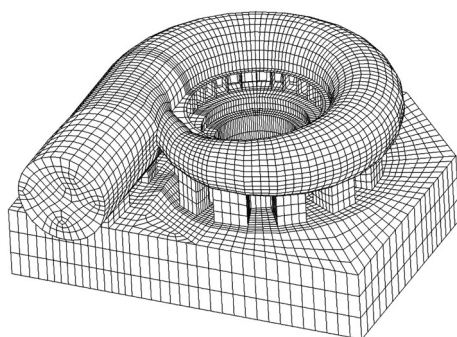
Fig. 6 First-stage concrete model
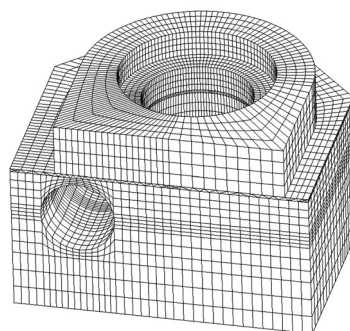
Fig. 7 Second-stage concrete model

These two models were simulated with 8-node reduced integration elements. The steel liner, stay vane, and stay ring of the spiral case were simulated with 4-node reduced integration elements. The steel bars were simulated with truss elements. The thickness of the steel liner decreased from 70 mm at the inlet to 32 mm of the tail tube.

The fixed boundary condition was applied to the bottom of the models, and the free boundary conditions were applied to the joints of the generator units. The nonlinear contact was assumed between the steel liner and concrete. It was considered that the pressure in the normal direction could be transferred through the contact areas, and that the pressure in the

tangent direction could be simulated with the penalty function and bond-slip model. The material parameters of the model can be seen in Table 1, and the data of standard concrete were adopted.

4.2 Constitutive relations and load analysis

The function of steel bars was simulated by embedding truss elements into concrete elements. The degrees of freedom for the neighboring nodes of steel bar elements and concrete elements were coupled in this method. According to the displacement coordination, the contribution of steel bars and concrete to the element stiffness matrix could be acquired, and a comprehensive element stiffness matrix was formed. A plastic model was used to simulate the mechanical properties of steel bars. The damage plasticity of concrete was considered to be independent of steel bars. On the assumption that concrete was nondestructive before it cracked, the interface cracking effect was simulated by tensile softening and adjusting the stiffness matrix. The tensile damage variation curves of concrete can be seen in Fig. 8.

(a) Tensile stress of concrete   (b) Damage properties of concrete
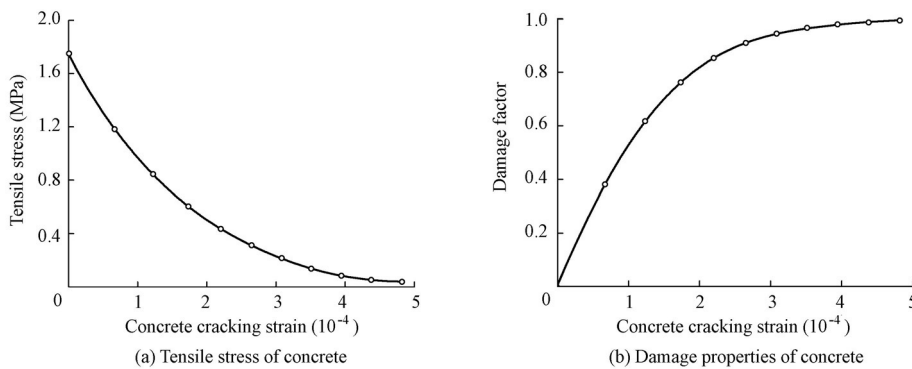
Fig. 8 Cracking properties of concrete

The loads included the structure weight, the weights of the stationary parts and rotational parts (generator rotor, spindle, runner, etc.) of the generator unit, the concentrated force on the stay ring (95 638 kN), the live load (20 kPa), the load of the first-stage concrete (1.80 MPa), and the load of the second-stage concrete (2.8 MPa).

5 Results and discussion

5.1 Steel liner stress

Some sections such as the 0°, 90°, 180°, and 270° sections were selected at several positions in the direction of water flow. The feature points of each section are displayed in the sequence from *A* to *I* around the circumference of the spiral case, as shown in Fig. 9.

The results of the steel liner equivalent stresses of
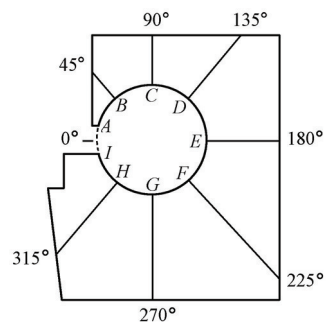
Fig. 9 Positions of feature points

characteristic sections derived from the simulation algorithm, the simplified algorithm, and the shell-spring algorithm under the load of 2.8 MPa were compared, as shown in Fig. 10. The trends of stress distribution are similar. In each section, the stress decreases gradually from point *A* to point *C*, and then to point *E*. It then increases from point *E* to point *G*, and continues to increase toward point *I*. The maximum stress obtained by the shell-spring algorithm is the highest of the three methods, reaching 169.2 MPa.
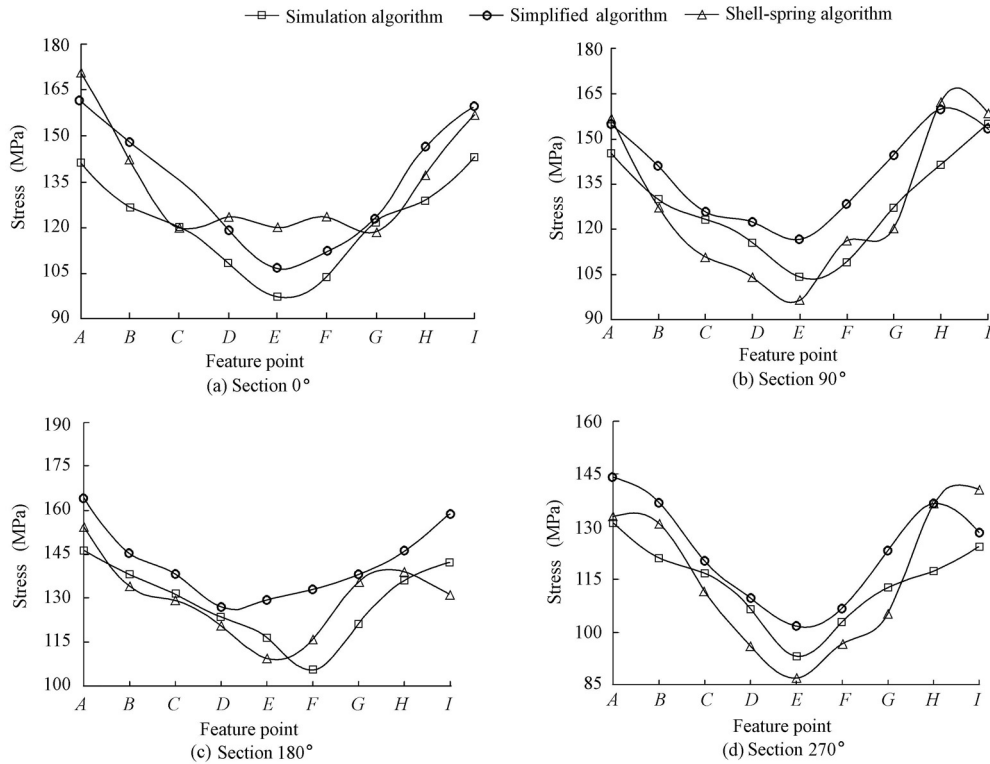
Fig. 10 Stress on different characteristic sections

It can be seen that the steel liner stress calculated with the simplified algorithm is higher than that of the simulation algorithm. The regularity of the results of the shell-spring algorithm is not as obvious as those of the simplified and simulation algorithms. The curves of the shell-spring algorithm are similar to those obtained by the simplified and simulation algorithms.

The results of the simulation algorithm were analyzed according to the practical construction and operational processes. If the three methods were evaluated from the perspective of the average hoop stress for the same section, the difference between the shell-spring algorithm and simulation algorithm was 11.01%, while the difference between the shell-spring algorithm and the simplified algorithm was only 8.69%. The results indicate that the shell-spring algorithm can reflect the stress of the steel liner to a certain extent.

5.2 Gap variation

The initial gap between the steel liner and concrete structure was formed by the specific

construction method. The gap openings calculated with the simulation algorithm are shown in Table 2. Gaps vary from the top to the waist because of the shrinkage of the steel shell after uneven pressure relief in the radial direction. The values of the initial gaps are from 0.21 mm to 3.68 mm. The initial gap openings near the bottom and buttress are less than 1.0 mm.

Table 2 Gaps under internal pressure

Section	Load (MPa)	Gap opening (mm)								
		A	B	C	D	E	F	G	H	I
0°	Initial	0.91	1.49	2.86	3.23	2.56	1.27	0.33	0.97	0.81
	1.8	0.32	0.01	0.23	0	0	0	0	0.14	0.52
	2.8	0	0	0	0	0	0	0	0.07	0.65
90°	Initial	0.31	1.85	3.68	3.12	2.23	0.91	0.51	1.19	1.13
	1.8	0.03	0.04	0.07	0	0	0	0	0.31	0.43
	2.8	0.01	0	0	0	0	0	0	0	0.41
180°	Initial	0.27	1.69	2.62	2.73	1.38	0.43	0.21	0.28	1.35
	1.8	0.06	0	0.03	0.07	0	0	0	0	0.23
	2.8	0	0	0	0	0	0	0	0	0
270°	Initial	0.21	1.10	2.07	1.95	1.07	0.34	0.29	0.31	0.43
	1.8	0.04	0	0	0.03	0	0	0	0	0.12
	2.8	0.13	0	0	0	0	0	0	0	0

The gap distributions are consistent with the data from the monitoring of the spiral case in the Three Gorges Project (Zhang and Liao 2007). As the boundary conditions change, such as the removing of bulkheads, the steel shell deformation will not stay the same as the previous value when the load reaches 1.8MPa, and some regional gaps are not closed tightly. When the load reaches 2.8 MPa, most gaps are narrowed. Only in the stay ring near the tip nose of the spiral case does gap disengaging occur.

Although it is assumed that the changes in gap openings are uneven when the simplified algorithm is used, the simplified algorithm is not suitable for practical engineering. As for the results obtained with the simulation algorithm, they are not always the same in the gap distribution in different sections. At points *E*, *F*, and *G*, the gap will close ahead even though the load does not reach the water head to maintain the internal pressure. The gap closing sequence among those points is *G→F→E→D→H→C→B*. The gap closing ahead means that concrete there bears loads together with the steel liner in advance, that is to say, the load-bearing ratio between the steel liner and concrete varies with the gap in between. This phenomenon cannot be reflected by the simplified algorithm. Therefore, the previously adopted simplified algorithm is not a safe way to design the power station.

5.3 Concrete plastic damage

In this study, with the simulation algorithm, the damage-plasticity model for concrete was

used to simulate the cracking characteristics of the surrounding concrete. The plastic damage to the whole structure is shown in Fig. 11, and the damage to each section can be seen in Fig. 12. Microcracks occur in regions with damage factors over zero, and the concrete macroscopic fracture occurs if the factor reaches 1.0.
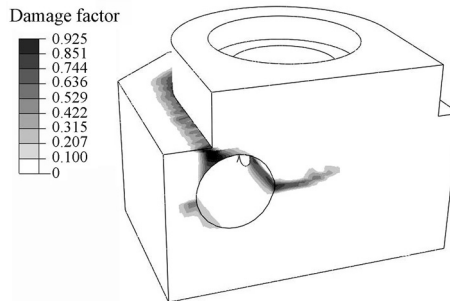
Fig. 11 Contour of tensile damage to concrete structure of spiral case

(a) Section 0°   (b) Section 90°   (c) Section 180°   (d) Section 270°
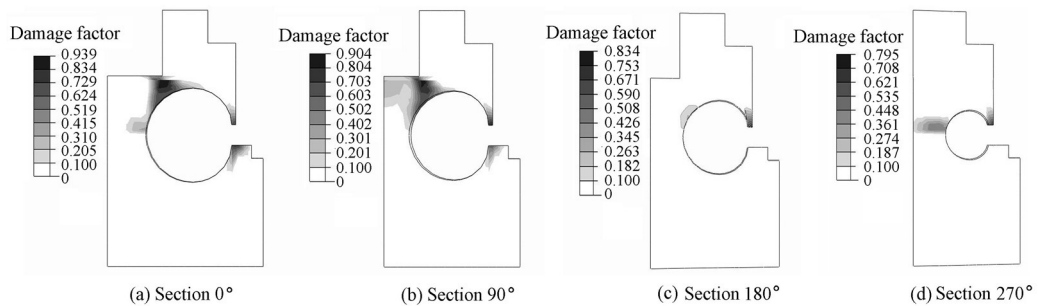
Fig. 12 Contours of tensile damage to different sections of concrete structure of spiral case

The most serious tensile damage appears at the interface between the concrete pier and the inlet portion of the spiral case. The damage factor reaches 0.94 in this region, meaning that the macroscopic fracture does not occur, and the whole structure is still in the safety condition. Some plastic damage appears inside and outside of the inlet along the horizontal direction, but the damage factor is smaller. As seen in Fig. 12, some places in the 0°, 90°, and 270° sections have large damaged areas. High damage factors are obtained in these places, and some damaged regions almost run through the whole concrete model. There is no serious damage to the 180° section, only some damages near the stay ring. The diameter of the spiral case decreases gradually along the tube in the flow direction, and the damage also decreases.

The damage evolution process in the 0° section of the surrounding concrete is shown in Fig. 13, which shows that the plastic damage to the stay ring appears as the load increases. The weakest portion of the whole concrete structure is in this section. When the load increases to 2.8 MPa, the tensile damage to the interface between the concrete pier and the inlet portion develops with the increase of the damage factor from 0.6 to 0.9, and the damage penetrates the top of the whole concrete structure. As a result of the extension of the plastic damage, a smaller region of damage occurs at the bottom of the stay ring, and gradually extends from the

inside to outside along the waist line.

(a) $P = 0.5$ MPa   (b) $P = 1.5$ MPa   (c) $P = 2.0$ MPa   (d) $P = 2.5$ MPa
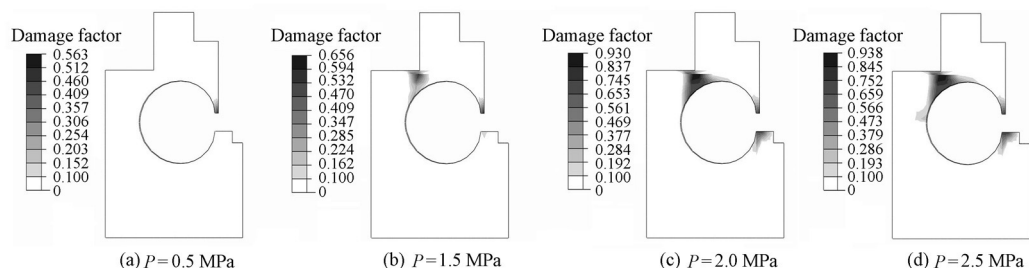
Fig. 13 Development of tensile damage at section 0° under different loads P

In this study, the impact of the concrete pier on the damage to the spiral case structure was investigated. From the results, it can be seen that serious damage appears on the interface between the concrete pier and the inlet portion. The results are different from Ma (2010), in which the pier effect was not considered, and cracks only occurred at the top of the structure. The present results are similar to the fracture distribution in the Three Gorges model experiment (Zhang and Liao 2007). In summary, the numerical calculation of structures using the damage-plasticity model for concrete is reliable for the structural analysis of spiral cases to a certain degree.

6 Conclusions

This paper proposes a numerical method to simulate the damage to the concrete structure of the spiral case. The method is an improvement of the simplified algorithm, and the conclusions are as follows:

(1) The simulation algorithm has confirmed the non-uniform variation of gaps between the steel liner and surrounding concrete. The load-bearing ratio between the steel liner and concrete is affected by the gaps in between. Concrete will bear the load before it reaches 2.8 MPa. These results are different from the previous simplified algorithm.

(2) Despite the damage occurring in the weak region and penetrating other regions of the concrete structure, the whole structure is sound. The tensile damage distribution is affected by the concrete pier in the model.

(3) The shell-spring algorithm presented in this paper can be used to conduct a reliable analysis of finite elements in an optimized way.

References

Burlion, N., Gatuingt, F., Pijaudier-Cabot, G., and Daudeville, L. 2000. Compaction and tensile damage in concrete: Constitutive modeling and application to dynamics. *Computer Methods in Applied Mechanics Engineering*, 183(3-4), 291-308. [doi:10.1016/S0045-7825(99)00223-6]

Chaboche, J. 1987. Continuum damage mechanics: Present state and future trends. *Nuclear Engineering Design*, 105(1), 19-33. [doi:10.1016/0029-5493(87)90225-1]

Del Rio, L., Barrie, R. E., Yeh, C. H., and Vig, V. 1991. Design of powerhouse spiral case considering three-dimensional action. Darling, D. D. ed., *Waterpower'91*: *A New View of Hydro Resources*, 801-809.

New York: ASCE.

Dong, Y. X., and Li, Y. S. 1995. *Structure Analysis of Hydroelectric Power Engineering*. Dalian: Dalian University of Technology Press. (in Chinese)

Hibbitt, Karlsson, and Sorensen Incorporation (HKSI). 2002. *ABAQUS/Standard User's Manual*. Providence: HKS Incorporation.

Lee, J., and Fenves, G. L. 1998. Plastic-damage model for cyclic loading of concrete structures. *Journal of Engineering Mechanics*, 124(8), 892-900. [doi:10.1061/(ASCE)0733-9399(1998)124:8(892)]

Li, W. F., Li, J. C., and Zhao, X. N. 2004. The study on stress simulation of the preloading filling spiral case of hydropower station. *Water Power*, 30(3), 52-54. (in Chinese)

Lin, S. Z., and Su, H. D. 2001. 3-D FEM analysis for surrounding concrete of steel spiral case keeping internal pressure during construction. *Journal of Hydraulic Engineering*, 32(1), 66-70. (in Chinese)

Lubliner, J., Oliver, J., Oller, S., and Oñate, E. 1989. A plastic-damage model for concrete. *International Journal of Solids and Structures*, 25 (3), 299-329. [doi:10.1016/0020-7683(89)90050-4]

Ma, Z. Y., He, P. C., Zhang, Y. L., and Zhang, H. Z. 2010. Nonlinear simulation analysis for preloading spiral case of keeping constant internal water pressure of hydropower station. *Journal of Dalian University of Technology*, 50(6), 1014-1019. (in Chinese)

Mazars, J. 1985. A description of micro and macroscale damage of concrete structures. *Engineering Fracture Mechanics*, 25(6), 729-737. [doi:10.1016/0013-7944(86)90036-6]

Mazars, J., and Pijaudier-Cabot, G. 1989. Continuum damage theory: Application to concrete. *Journal of Engineering Mechanics*, 115(2), 345-365. [doi:10.1061/(ASCE)0733-9399(1989)115:2(345)]

Qin, J. Z., Ma, S. D., Gong, G. Z., and Xiong, D. Y. 2002. Structural model test for surrounding concrete of steel spiral case keeping internal pressure. *Journal of Hydraulic Engineering*, 33(10), 33-38. (in Chinese)

Ragueneau, F., La Borderie, Ch., and Mazars, J. 2000. Damage model for concrete-like materials coupling cracking and friction, contribution towards structural damping: First uniaxial applications. *Mechanics Cohesive-Frictional Materials*, 5(8), 607-625. [doi:10.1002/1099-1484(200011)5:8<607::AID-CFM108> 3.0.CO;2-K]

Shen, Y., Wu, H. G., and Jiang, K. C. 2008. Research on preloading filling spiral case structure in large pumped storage power station. *Journal of Huazhong University of Science and Technology (Nature Science)*, 36(5), 97-99. (in Chinese)

Xu, X. Y., Li, M. Z., Ma, Z. Y., Zhang, H. Z, and He, P. C. 2009. Simulation and analysis of the constant internal pressure spiral case with non-uniform gap. *Journal of Hydroelectric Engineering*, 28(4), 75-80. (in Chinese)

Zhang, X. M., and Liao, M. J. 2007. The analysis of monitoring results of the spiral case of 10# turbine in left powerhouse in the process of the placement. *Science and Technology of West China*, (9), 24-26. (in Chinese)

Zhang, Y. L., Zhang, C. H., and Ma, Z. Y. 2009. Nonlinear FEM analysis on stress and strain of directly-embedded large-scale spirals. *Journal of Hydraulic Engineering*, 40(2), 220-225. (in Chinese)

(Edited by Ye SHI)